Differential Location of NKT and MAIT Cells within Lymphoid Tissue

Darryl N. Johnson
University of Melbourne
Zheng Ruan
University of Melbourne
Emma V. Petley
Peter MacCallum Cancer Centre
Sapna Devi
University of Melbourne
Lauren E. Holz
University of Melbourne
Adam P. Uldrich
University of Melbourne
Jeffrey Y. W. Mak
University of Queensland
Jyh Liang Hor
University of Melbourne
Scott N. Mueller
University of Melbourne
James McCluskey
University of Melbourne
David P. Fairlie
University of Queensland
Phillip K. Darcy
Peter MacCallum Cancer Centre
Paul A. Beavis
Peter MacCallum Cancer Centre
William R. Heath
University of Melbourne
Dale I. Godfrey (godfrey@unimelb.edu.au)
University of Melbourne

Research Article

Keywords: Natural Killer T (NKT) cells , Mucosal-Associated Invariant T (MAIT) cells , lymphoid tissue, T cell receptors (TCRs)

Posted Date: August 6th, 2021

DOI: https://doi.org/10.21203/rs.3.rs-750259/v1

Version of Record: A version of this preprint was published at Scientific Reports on March 8th, 2022. See the published version at https://doi.org/10.1038/s41598-022-07704-4.

Abstract

Natural Killer T (NKT) cells and Mucosal-Associated Invariant T (MAIT) cells are innate-like T cells that express semi-invariant αβ T cell receptors (TCRs) through which they recognise CD1d and MR1 molecules, respectively, in complex with specific ligands. These cells play important roles in health and disease in many organs, but their precise intra-organ location is not well established. Here, using CD1d and MR1 tetramer staining techniques, we describe the precise location of NKT and MAIT cells in lymphoid and peripheral organs. Within the thymus, NKT cells were concentrated in the medullary side of the corticomedullary junction. In spleen and lymph nodes, NKT cells were mainly localised within T cell zones (TCZ), although following *in vivo* activation with the potent NKT-cell ligand α-GalCer, they expanded throughout the spleen. MAIT cells were clearly detectable in Vα19 TCR transgenic mice and were rare but detectable in lymphoid tissue of non-transgenic mice. In contrast to NKT cells, MAIT cells were more closely associated with the B cell zone (BCZ) and red pulp (RP) of the spleen. Accordingly, we have provided an extensive analysis of the *in situ* localisation of NKT and MAIT cells and suggest differences between the intra-organ location of these two cell types.

Introduction

Natural Killer T (NKT) and Mucosal Associated Invariant T (MAIT) cells are two distinct classes of unconventional αβ T cells that recognise non-peptide antigens in complex with MHC class-I-like molecules. Type I (sometimes known as invariant) NKT cells express a semi-invariant TCRα chain (Vα14Jα18 TCRα in mice; Vα24Jα18 in humans) that pairs with a biased pool of TCRβ chains through which they recognise self and foreign glycolipids presented in complex with CD1d [1]. The prototypical antigen recognised by type I NKT cells is the microbial antigen α-galactosylceramide (α-GalCer) [2]. Similar to NKT cells, MAIT cells also express an invariant TCRα chain (Vα19Jα33 in mice; Vα7.2Jα33 in humans) paired with an oligoclonal pool of TCRβ chains [3–5]. Unlike NKT cells however, MAIT cells recognise microbial-derived vitamin B2-based metabolites, such as 5-OP-RU (5-(2-oxoproylideneamino)-6-D-ribitylaminouracil), presented in complex with MR1 molecules [3–5]. Following activation, NKT cells and MAIT cells rapidly produce a broad range of cytokines and play protective roles against microbial infections and cancers as well as pathogenic effects in autoimmune and allergic diseases [1,5]. However, our knowledge of the *in situ* locations of NKT cells and MAIT cells is very limited.

NKT and MAIT cells develop in the thymus and migrate to the periphery, where they can be found in a broad range of both secondary lymphoid and peripheral tissues and organs including liver, intestines, lungs, skin, adipose tissue and other sites [5,6]. Early studies to identify NKT cells *in situ* used a CXCR6-GFP reporter system because NKT cells were highly enriched within the CXCR6-GFP$^+$ fraction of T cells. This reporter was used to visualise NKT cells patrolling liver sinusoids and interacting with Kupffer cells [7,8], responding to *Borrella burgdorferi* in knee joints[9] or residing in the medulla of LNs [10]. A limitation with this system is that not all CXCR6-GFP$^+$ cells are NKT cells and not all NKT cells express CXCR6-GFP [8]. Adoptive transfer of CFSE-labelled Vα14 transgenic NKT cells into non-transgenic C57BL/6 (B6)

recipients provided some of the first images of NKT cells which were detected in LN paracortex and splenic T cell zones (TCZ) of the white pulp (WP) [11,12]. However, it is unclear whether adoptively transferred TCR transgenic NKT cells will migrate and localise to the same sites as endogenous non-transgenic NKT cells. Immunohistology staining for a combination of CD3 or TCRβ and NK1.1 allowed for the first description of endogenous NK1.1$^+$ T cells and located these cells predominantly to the red pulp (RP) and marginal zone of the spleen[13] and liver sinusoids[14]. A limitation with this approach is the fact that not all NK1.1$^+$ T cells are NKT cells and not all NKT cells are NK1.1$^+$ [15]. CD1d-α-GalCer tetramer staining is the best way to accurately identify NKT cells and has been used with immunohistology to detect endogenous NKT cells in Vα14 TCR transgenic mice where NKT cells are highly abundant [16]. More recently, this approach has been used to detect endogenous NKT cells in thymus, spleen, lymph nodes and adipose tissue [17–20]. Within thymus, most NKT cells were detected throughout the medulla. In peripheral lymphoid organs, the location of NKT cells may be strain dependent. Thus in the spleen of C57BL/6 (B6) mice, most NKT cells were found in the RP, while conversely, in the BALB/c spleen, the major location of NKT cells shifted towards the TCZ [17,18]. Similarly, CD1d tetramer staining has located NKT cells within the LN follicle [18] or intrafollicular space [19] in B6 mice, but paracortex in BALB/c mice[18]. Thus, discrepancies between reports on of NKT cell locations in peripheral organs may reflect differences in the techniques for detection as well as strain-dependent differences in location of NKT cell subsets.

In the case of MAIT cells, immunohistological staining for CD3, CD8, Vα7.2, CD161 and/or IL-18R has been used to study MAIT cells in human liver [21–25], intestine[22,26–29], pancreas[30], brain[31–33] and lymph nodes[22] in either heathy or diseased states. However, these surrogate markers are not limited to MAIT cells[5], so it is difficult to know if the cells detected were MAIT or MAIT-like cells. Recently, direct MAIT cell staining with MR1-5-OP-RU tetramer, the gold standard for MAIT cell detection, was used to detect MAIT cells in mouse lung, a site with a high proportion of MAIT cells, following *Legionella longbeachae* infection [34]. The location of MAIT cells, defined by MR1-5-OP-RU tetramer, in other tissues remains unknown.

Because there remains great uncertainty about the *in situ* localisation of NKT and MAIT cells, in this study, we have investigated this problem using CD1d-α-GalCer and MR1-5-OP-RU tetramers, which are the gold standard for identifying NKT and MAIT cells, in a range of different mouse tissues, including appropriate control tetramers and CD1 and MR1 deficient mice, to increase confidence that the cells detected are indeed NKT and MAIT cells. We have clarified and expanded upon previous studies in terms of NKT cell location, including following *in vivo* activation and compared the locational differences between NKT cells and MAIT cells in secondary lymphoid organs.

Results

Identification of endogenous NKT cells in situ with α-GalCer loaded CD1d tetramers.

We have used CD1d tetramer for immunohistological analysis of NKT cells in a range of mouse tissues. To validate the specificity of our approach, fresh frozen spleen sections from BALB/c wild type (WT) or BALB/c.CD1d$^{/-}$ mice were stained with CD1d tetramers loaded with α-GalCer or left unloaded (presumably carrying endogenous lipids) (Fig. 1a and Supplementary Fig S1). Within the WT spleen, cells could be identified that had clearly bound the α-GalCer-loaded CD1d tetramer with limited staining observed on WT sections stained with the unloaded CD1d tetramer or CD1d$^{-/-}$ mouse spleen sections stained with CD1d-α-GalCer tetramer. Though, in all three groups, we observed rare examples of CD1d tetramer staining that appeared not to associate with the TCRβ stain (Supplementary Fig S1b), thus the co-localisation of CD1d tetramer and TCRβ was investigated. Voxel plots of the three groups indicated a clear association within BALB/c WT sections of voxels stained with CD1d-α-GalCer and TCRβ (Supplementary Fig S1c). Analysis of Pearson's correlation and the area co-stained by CD1d-α-GalCer tetramer and TCRβ both indicated a positive correlation between CD1d-α-GalCer and TCRβ staining on WT sections compared to negative control stained sections (Supplementary Fig S1d and e). Taken together, these data highlight the ability of the CD1d-α-GalCer tetramers to specifically stain endogenous NKT cells *in situ*. Importantly, they also demonstrate the need to co-stain with T cell specific markers such as TCRβ or CD3 and include negative controls for stain and tissue to best eliminate, albeit rare, non-NKT cell staining from analysis.

Having established the technique to reliably identify NKT cells *in situ*, we next examined the location of NKT cells in primary and secondary lymphoid organs. On average, roughly 100 NKT cells per field of view could be observed within BALB/c spleen (Fig. 1b), the majority (~ 70%) of which were found within the TCZ rather than the BCZ or RP (Fig. 1c). Within these regions, NKT cells were scattered either alone or in small clusters. We also examined spleens from C57BL/6 (B6) mice and detected roughly 40 NKT cells per field of view (Supplementary Fig S2a and b). There was also a clear difference in the location of NKT cells between the two stains of mice. Where in the spleens of B6 mice, more NKT cells were found in the RP with the remaining NKT cells in roughly equal proportions in the TCZ and BCZ (Supplementary Fig S2c). In spleens from both BALB/c and B6 mice, we detected some CD1d tetramer^{+} cells that are not likely to be NKT cells because they did not co-stain for CD3/TCR. Similar infrequent staining was observed in CD1d$^{-/-}$ spleens and WT spleens stained with CD1d tetramer loaded with an irrelevant glycolipid antigen, disialoganglioside (GD3) (Fig. 1a, Supplementary Fig S2d).

The distribution of NKT cell subsets in BALB/c mice was also investigated based on the expression or absence of CD4, which defines many, but not all NKT cells, as shown by flow cytometry (Fig. 1d). In general, CD4 expression in the spleen was observed throughout the organ, though as expected the greatest concentration of expression was associated with CD3 within the TCZ (Fig. 1e), representing conventional CD4 T cells. Using colocation analysis between CD3^{+}CD1d-α-GalCer^{+} and CD4^{+} stains to separated NKT cells into CD4 expressor and non-expressor channels, the distribution of CD4^{+} and CD4^{-} NKT cells could be determined (Fig. 1f). Interestingly, while the majority (~ 75%) of NKT cells within the TCZ expressed CD4, there were roughly equal proportions of CD4^{+} and CD4^{-} NKT cells within the RP or BCZ expressed this marker (Fig. 1g). These data suggest that there is differential distribution of NKT

$CD4^+$ and $CD4^-$ subsets may reflect differential expression of chemokine receptors or adhesion molecules [35,36].

Within peripheral (brachial) lymph nodes (LN) there were far fewer NKT cells observed per field of view than in spleen sections, nonetheless, compared to negative controls NKT cells could still be observed (Fig. 2a and b). By scanning multiple sections, we were able to determine that the majority of NKT cells were localised within the paracortex rather than the medulla or B cell follicles of lymph nodes (Fig. 2c).

The location of NKT cells in thymus was examined by costaining for thymic cortical and medullary regions using CD205, cytokeratin 5 and CD3 and CD1d-α-GalCer (Fig. 3a and b). This demonstrated that, consistent with previous reports [18] the vast majority of NKT cells were located within the medulla. Furthermore, the medullary NKT cells tended to localise close to, or within, the corticomedullary junction (CMJ) as a higher density of these cells were observed within 100 μm of the CMJ (Fig. 3c). Thymic NKT cells can also be subdivided into $CD4^+$ and $CD4^-$ fractions, as shown by flow cytometry (Fig. 3d) and immunohistology (Fig. 3e). Following co-localisation analysis (Fig. 3f and 3g), we found that within both thymic regions most NKT cells expressed CD4 (~ 75% within the cortex and ~ 60% within the medulla).

These results demonstrate that NKT cells occupy specific locations within the primary and secondary lymphoid organs and, for the most part, they are located in similar regions to conventional T cells in BALB/c mice. We have also shown that while NKT can be divided into CD4 + and CD4- subsets, for the most part both populations were intermingled, although there were some differences in the ratio of these subsets in different locations.

Thymic medullary structure in mice lacking NKT cells.

A recent study showed that emigration of mature thymocytes from the thymus was dependent on the type-2 cytokine receptor IL-4Rα chain [37]. Lack of IL-4Rα and impaired thymic emigration led to accumulation of mature thymocytes in the medulla around perivascular spaces, leading to the formation of large medullary areas devoid of epithelial stromal cells. Moreover, this study also showed the appearance of these medullary epithelial cell-free areas in CD1d-deficient mice, suggesting a key role for NKT cells as a source of IL-4 that regulates thymic emigration[37]. CD1d-deficient mice lack both type I and type II NKT cells, both of which can produce IL-4 and IL-13. Therefore, we sought to explore if these epithelial cell-free areas (that we refer to as voids) were specifically due to the lack of type I NKT cells by comparing medullary thymic epithelial cell staining in WT, $CD1d^{-/-}$ and $Jα18^{-/-}$ thymuses (the latter deficient in type I but not type II NKT cells). While we were able to detect some areas in the medulla that were devoid of thymic epithelial cells (as outlined with green line) (Fig. 4a), these did not resemble the clear ring like structures that were previously reported[37]. Moreover, we found no significant difference in the number of voids in $CD1d^{-/-}$ (Fig. 4b) and while the average size of these was marginally increased in $CD1d^{-/-}$ mice, this was also not significant (Fig. 4c). We also failed to detect any increase in the size of medullary holes in type I NKT cell deficient $TCRJα18^{-/-}$ mice. As these data were acquired in B6 strain

background, we also carried out similar studies in BALB/c mice where NKT cells produce higher levels of IL-4, but again, we were unable to detect a clear increase in the appearance of medullary voids (Supplementary Fig S3). As a positive control for detection of medullary epithelial cell voids, we also tested thymuses from NOD mice, as these are known to contain large numbers of B cells in the thymic medulla that lead to enlarged perivascular spaces that disrupt thymic epithelial structure [38]. Clear evidence of medullary voids were detected in NOD mouse thymi (Fig. 4a). Another consideration was that CD1d-deficient mice have increased MAIT cells, particularly on the BALB/c background [39]. Therefore, we also examined Vα19 TCR transgenic.Cα$^{-/-}$ mice (Vα19Tg) and MR1$^{-/-}$ mice, which have increased, and decreased, MAIT cells respectively [40,41] for medullary voids, but these were also not significantly different from control B6 mice (Supplementary Fig S3). Taken together, while we have confirmed the presence of NKT cells in the thymic medulla, we have been unable to verify that the absence of any thymic NKT cell population has an impact on thymic medullary architecture.

In situ observation of NKT cells in peripheral organs.

As well as primary and secondary lymphoid organs, NKT cells reside in a range of non-lymphoid organs, particularly in the liver, small intestines and lungs. Thus, we endeavoured to detect NKT cells in a range of peripheral organs using CD1d tetramer staining. While CD1d-α-GalCer tetramer^{+} cells were detected within the small intestine, lungs, kidneys and heart of BALB/c WT mice (Supplementary Fig S4 to S7), many of these stained brightly with the tetramer, but not with CD3. Furthermore, the importance of the unloaded CD1d tetramer control stain was highlighted by the existence of CD3^{-} cells that bound to unloaded CD1d tetramer in these tissues. For example, in the small intestine non-specific (CD1d tetramer positive, but CD3 negative) staining could be observed prominently in the villi, regardless of whether CD1d was loaded with negative control antigen (Supplementary Fig S4a) or α-GalCer (Supplementary Fig S4b). Similarly, in the lung (Supplementary Fig S5), kidney (Supplementary Fig S6) and heart (Supplementary Fig S7), GD3 and α-GalCer loaded CD1d tetramer positive, but CD3 negative staining could be also observed. Importantly, despite these non-specifically stained cells, CD3^{+}CD1d/α-GalCer^{+} cells were also detected, albeit infrequently, in Payers Patch (Supplementary Fig S4b) and the villi (Supplementary Fig S4c) of small intestine. Rare NKT cells were detected in the lungs within the alveolar ducts (Supplementary Fig S5b). In kidney, NKT cells could be observed between convoluted tubules (Supplementary Fig S6b) and in the heart within the myocardium between perimysical septa (Supplementary Fig S7b). Because NKT cells were so infrequent in lung, kidney and heart (1–4 per section), it was difficult to determine their preferred location.

Relocation of NKT in the spleen following α-GalCer stimulation.

Having demonstrated the *in situ* location of NKT cells in lymphoid tissues, we next examined what happened to the location of these cells following *in vivo* activation. Mice were injected intraperitoneally with 2μg α-GalCer and the expansion of NKT cells was determined on days 3 and 5 post injection. As expected, FACS analysis of spleen cell suspensions from these mice showed a rapid increase in NKT cell numbers in the spleen 3 days post injection, which decreased by day 5 post injection (Fig. 5a and b). This was also reflected by a clear increase in CD1d-α-GalCer tetramer staining of spleen tissue sections taken at day 3 after activation, and subsequent reduction in the extent of this staining at day 5 (Fig. 5c and d). As expected CD1d-α-GalCer staining was associated with CD3 staining (Supplementary Fig S8). As previously shown, $CD3^+CD1d\text{-}\alpha\text{-}GalCer^+$ NKT cells in unstimulated mice were observed throughout the spleen with largely equal proportions of NKT cells in the BCZ and RP, while most (~ 10x as many) were located within the splenic TCZ. By day 3 following antigen stimulation, the proportion of NKT cells in all three regions increased, and some redistribution of NKT cells was apparent by day 5 (Fig. 5e). While NKT cells within the TCZ remained the largest population, increasing ~ 2.5-fold 3 days post stimulation, the BCZ saw the greatest increase in NKT cell density such that by day 3, the population of NKT cells in this region had increased ~ 7-fold. We also observed a ~ 3-fold increase in the frequency of NKT cells within the RP 3 days following stimulation. By day 5, the frequency of $CD3^+CD1d\text{-}\alpha\text{-}GalCer^+$ NKT cells in the TCZ and RP had declined to levels that were similar to unstimulated mice. In contrast, the frequency of cells in the BCZ remained ~ 2.8-fold higher compared to unstimulated mice. The increased $CD3^+CD1d\text{-}\alpha\text{-}GalCer^+$ NKT cells within the BCZ may reflect their role in modulating B cell responses following activation.

We next investigated NKT cells in the periphery following stimulation. The liver is a major non-lymphoid organ known to contain a large population of NKT cells. Following injection of α-GalCer, an expanded population of NKT cells was detected that followed a similar expansion pattern as in the spleen; a large expansion 3 days post stimulation, which had contracted by day 5 (Supplementary Fig S9a and b). Detecting NKT cells in situ in this organ proved challenging due to its large size, and low frequency of lymphocytes in general; nonetheless, NKT cells were detected, albeit infrequently, within the liver sinusoids. Consistent with the cytometry data, NKT cells were more frequent at day 3 where it was possible to observed 2–7 NKT cells per field of view. In livers of either unstimulated or day 5 post challenge mice, however, they remained difficult to locate (1–3 per section). Importantly, regardless of the time point, these cells co-stained with CD3 and this staining was not observed in negative control sections (Supplementary Fig S9c).

Multiparameter histo-cytometry of splenic NKT cells, T cells, B cells and antigen-presenting cells.

The cellular environment within lymphoid organs is complex and involves many different subsets of immune cells each influencing the actions of the others. Indeed, NKT cells interact with and modulate the responses of a range of innate and adaptive immune cells [42]. These varying cell types are difficult to investigate together with typical histological techniques due to lack of methods to stain for the multitude

of cell surface receptors required to fully identify the diverse array of immune cells *in situ*. Therefore, we used multiparameter histo-cytometry [43] to visualise NKT cells in the context of other immune cells. To this end, spleen sections were stained with a range of cell surface receptors (CD11c, CD11b, CD3, CD4, CD1d/α-GalCer, B220 and MHC-II) and cell nuclei with DAPI and the separate fluorescence of each stain was determined by spectral unmixing and compensation (Fig. 6a and Supplementary Fig S10a). Cells were segmented based on the DAPI strain (Supplementary Fig S10b) and separate cell populations determined by conventional cytometry analysis (Fig. 6b). Clear populations of B cells and T cells as well as NKT cells and various APC populations could be identified and were plotted back to cells within the image and the original stains (Fig. 6c). CD4 positive and negative T and NKT cells proved difficult to separate using this technique, likely owning to their being closely packed and intermingled in the similar spatial location, namely the TCZ. Overall, however, the various cell populations could be mapped within the same histological regions within the spleen as they were observed in the original stained sample (Supplementary Fig S10d), but with greater clarity, providing a better way to analyse these cells in association with other diverse cell types. This approach supports our previous observations that NKT cells were largely located within the TCZ, of which most were $CD4^+$ (Fig. 6d, zoom panels III, VI and VII), while a small number of $CD4^-$ NKT cells were found in the BCZ (Fig. 6d, zoom panels V and IX) and RP (Fig. 6d, zoom panels IV and VIII). Some NKT cells were also found in marginal zone (Fig. 6d, zoom panels V and VII). As expected, a majority of the APCs were observed outside the white pulp with macrophages prominent throughout the RP, while $CD11b^-$ and $CD11b^+$ DCs mostly associated with the marginal zone (Fig. 6d, zoom panels IV, V, VII and VIII). In particular, $CD4^-$ NKT cells were observed in amongst the $CD11b^-$ DCs (Fig. 6d zoom panel IV and V).

In situ identification of MAIT cells with MR1-5-OP-RU tetramers.

Very little is known about the location of MAIT cells within tissues. Similar to the technique to stain for NKT cells, MR1 tetramers loaded with MAIT cell-specific antigen 5-OP-RU were used to identify MAIT cells. MAIT cells are much rarer than NKT cells in mice [41] so to begin with, we used the Vα19Tg mice, which contain a much larger proportion of MAIT cells than WT mice. A clear population of brightly stained MR1-5-OP-RU $tetramer^+$ $CD3^+$ T cells was observed in spleen, lymph nodes and thymus of Vα19Tg mice. Importantly, this staining was not evident on sections stained with control acetyl-6-formylpterin (Ac-6-FP)-loaded MR1 tetramer (Fig. 7), supporting the specificity of this staining for MAIT cells. In all organs, the pattern of MR1-5-OP-RU tetramer staining in the Vα19Tg mice was similar to that observed for NKT in WT mice, with the major difference being the greater number of MAIT cells observed in the Vα19Tg mice. In spleen, MAIT cells were mainly detected in the TCZs and less frequent cells were detected in the BCZs and RP (Fig. 7a). Similarly, MAIT cells were prominent in the LN paracortex, though unlike NKT cells, MAIT cells were also observed in the Vα19Tg LN medulla (Fig. 7b). Curiously, non-specific staining in the region of the glass slide where OCT was located was consistently observed with the 5-OP-RU loaded MR1 tetramer, but not MR1-Ac-6-FP (Fig. 7b and S13a). The reason for this effect is

unknown but may be a result of the natural fluorescence of 5-OP-RU [44]. In the thymus, the vast majority of MAIT cells were detected in the thymic medulla (Fig. 7c). These results show that, similar to the identification of NKT cells with CD1d-α-GalCer tetramers, MAIT cells can also be observed *in situ* with the use of MR1-5-OP-RU tetramers.

Next, we examined the location of MAIT cells in non-TCR transgenic C57BL/6 (B6), BALB/c and B6-$MAIT_{CAST}$ (CAST) mice (Fig. 8 and Supplementary Fig S11). The latter were also tested because this congenic strain is reported to have an increased number of MAIT cells, due to increased intrathymic selection of these cells [45]. While infrequent, nonetheless, MAIT cells could be readily observed in spleens stained with MR1/5-OP-RU tetramer in all three mouse strains. Importantly, these cells were not detected in the spleens from B6, BALB/c or CAST mice when stained with MR1/Ac-6-FP, nor were they detected in B6.$MR1^{-/-}$ or CAST.$MR1^{-/-}$ mice stained with MR1-5-OP-RU tetramer (Fig. 8b, S11b and e). Furthermore, MR1/5-OP-RU staining associated with CD3 staining. Similar numbers of MAIT cells (~ 10–20 cells) were observed in the spleens of B6 and CAST mice, while in BALB/c spleen only 5 cells on average could be observed. Interestingly, and in contrast to MAIT cells in the Vα19Tg mice, for each of the non-transgenic strains tested, most of the MAIT cells were detected outside the TCZ; collectively within the BCZ and RP of the spleens (Fig. 8c and S11c and f). We also attempted to investigate the locational differences between the NKT cells and MAIT cells by co-staining spleen sections of B6 and BALB/c mice with both CD1d-α-GalCer and MR1-5-OP-RU tetramers (Supplementary Fig S12a and b). A challenge with this approach is that both tetramers work optimally using the same fluorochrome, so a suboptimal fluorochrome was used for CD1d-α-GalCer tetramer staining. Furthermore, MAIT cells were more readily detectable in B6 mice while NKT cells were more detectable in BALB/c mice, so both were tested. Nonetheless, this co-staining supported the concept that NKT cells and MAIT cells occupy different locations in spleen. The thymuses of all three strains of mice were also stained with MR1-5-OP-RU tetramer (Supplementary Fig S13a to c). While a very small number of MR1/5-OP-RU + $CD3^+$ cells could be seen in the cortex of the thymus of B6 and CAST mice, they were undetectable in BALB/c mice. This is not surprising because we have previously published MAIT cells are exceedingly rare in mouse thymus [41]. Furthermore, a similar number of MR1 $tetramer^+$ but $CD3^-$ cells were also observed in negative controls, which again highlights the importance of appropriate controls in attempting to detect MAIT cells *in situ*. Nevertheless, with appropriate caution based on detection of very few cells, this suggests that MAIT cells may preferentially reside in the cortex of the thymus of non-Vα19 TCR transgenic mice, in contrast to their medullary location in Vα19 TCR transgenic mice (Fig. 7c).

The distribution of MAIT cells following *in vivo* activation was investigated by intranasal (i.n.) administration of 5-OP-RU in CAST mice and MR1-5-OP-RU tetramer staining of mediastinal LN (Supplementary Fig S14). Similar to the MR1 tetramer staining in the spleen, while only a small number of MAIT cells could be observed in these LNs, these were not detected than when the same tissue was stained with negative control Ac-6-FP loaded MR1 tetramer. Not-withstanding the small numbers of MAIT cells detected, there appeared to be an increase in their abundance following 5-OP-RU challenge

(Supplementary Fig S14c) and most were located within or on the edge of the paracortex (Supplementary Fig S14b and d).

While interpretation of these data is limited by the scarcity of cells detected in non-TCR transgenic mice, these results suggest that MAIT cells in WT mice occupy specific locations within lymphoid tissues, primarily located in regions of the spleen that differ from NKT cells and conventional T cells and that this is not reflected by the location of MAIT cells in TCR transgenic mice.

Discussion

This report examines the location of both NKT cells and MAIT cells *in situ* using CD1d-α-GalCer and MR1-5-OP-RU tetramers, respectively. These reagents are widely used in flow cytometry, but very few studies have employed them for *in situ* detection of NKT and MAIT cells. We demonstrate the feasibility of using these reagents to identify NKT and MAIT cells *in situ*. We also emphasise the need to include appropriate controls, such as GD3-loaded CD1d tetramers; Ac-6-FP-loaded MR1 tetramers; and CD1d and MR1 deficient mice, respectively. This was in order to identify false-positive staining that we demonstrate can sometimes be as abundant as the actual NKT and MAIT cells. The basis for this false positive staining is unknown, but it is also observed by flow cytometry [41,46] where tetramers can stain non-T cells. In these flow cytometry settings, co-labelling of CD1 and MR1 tetramers is usually accompanied at least by anti-TCR or anti-CD3 antibodies to ensure that T cells are being analysed.

Previous attempts at *in situ* tetramer staining showed how challenging this approach is. Indeed, the first reported use of CD1d-α-GalCer tetramer *in situ* successfully stained NKT cells in Vα14 transgenic mice where these cells are abundant but could not accurately detect them in non-transgenic settings [16]. Within the Vα14 transgenic mice, NKT cells were observed in the TCZ of the spleen and lymph nodes. More recently, some studies have succeeded in using CD1d-α-GalCer tetramers to identify NKT cells in non-transgenic mice [17–20], although as we demonstrate in this study, non-specific CD1d-tetramer staining may complicate interpretation. In our hands, this type of non-NKT staining was associated within both the RP and BCZ. Therefore, without specifically defining NKT cells with tetramer and CD3 or TCR staining it remains a possibility that in previous studies some non-NKT cell staining has given the impression that a higher proportion of NKT cells exist in the BCZ and RP. Furthermore, the varying methods of tetramer staining themselves have the potential to influence results. Previous investigations using CD1d tetramer have taken a whole tissue staining approach [18–20] where whole segments of tissue are immersed in the stain and the tetramer diffuses passively into the specimen. A possible problem with this approach could be uneven staining particularly in the deeper white pulp where tetramer penetration may be limited. Indeed, incomplete tissue absorption can be an issue even for some antibodies in techniques that stain whole tissue segments [47]. In contrast, we have stained thin tissues sections directly with the tetramer ensuring that NKT cells are evenly stained across the section.

Early investigations into the location of NKT cells in the spleen and lymph node have relied on staining for surrogate markers such as NK1.1 or CXCR6-GFP reporter, sometimes combined with adoptive transfer

of labelled NKT cells [8,10,12,13]. These studies point towards the lymph node medulla and splenic RP and MZ as the location of the majority of NKT cells in these organs. However, neither of these approaches exclusively label NKT cells, and furthermore, not all NKT cells express NK1.1 or CXCR6 [8,10]. Therefore, some or most cells identified might not be NKT cells and some NKT cells would likely be missed from the analysis. Furthermore, adoptive cell transfer may activate NKT cells and hence affect the locations they traffic to post transfer. Indeed, in contrast to studies using NKT cell transfer, the first studies to use *in situ* CD1d-αGalCer tetramer staining primarily located resting NKT cells in the splenic TCZ [16,17]. Using a CD1d-α-GalCer tetramer-based approach, we investigated the location of NKT cells in the spleens of BALB/c and B6 mice. The strain-specific differences we observed, where most NKT cells were localised in the TCZ, and occasionally in the B cell follicles of the WP in BALB/c mice, versus a RP location in B6 mice, is in line with a previous study [18]. In the spleens of both mouse strains, NKT1 cells were localised mostly outside the splenic WP, while most NKT2 cells were found within the WP[18]. Thus, the strain-specific differential location we observed may be explained by the fact that NKT2 cells are more abundant in BALB/c than B6 mice [48]. This may also explain our finding by colocalization analysis and histo-cytometry that $CD4^+$ NKT cells were more frequent in the TCZ, because all NKT2 cells express CD4 whereas NKT1 cells can be $CD4^+$ or $CD4^-$ [48,49].

While NKT cells were mainly in the TCZ rather than the BCZ of unstimulated BALB/c mice, a large increase in BCZ NKT cells was observed 3 days following α-GalCer mediated *in vivo* NKT cell activation. NKT cells are well known to provide B cell help through germinal centre formation, antibody class switching and affinity maturation [19,50–52]. Depending on the infection and mode of activation, NKT cells can provide both cognate and non-cognate help to B cells. For instance, NKT activated in response to α-GalCer modulate B cell response in a CD1d-TCR dependent manner [50–52], while during viral infection, activated NKT cells can influence B cell responses in a non-cognate fashion via the production of cytokines such as IL-4[19]. Previously, tetramer staining has been used to investigate NKT cell non-cognate B cell help during influenza virus infection [19]. It was seen that early in infection NKT cells migrated to the B cell border in the mediastinal LN and provided non-cognate B cell help via the local production of IL-4. Similarly, within 4 hours following intravenous antigen injection tetramer staining has shown that NKT cells rapidly migrate to the splenic MZ where they interact with MZ DCs and express IL-4 [17]. We similarly saw the expansion and change in the location of NKT cells in the spleen following activation, though in contrast, by day 3 following α-GalCer injection we observed that a large proportion of NKT cells resided in the BCZ. B cells are capable of presenting α-GalCer to NKT cells [50,52]. It is possible that following early migration to the MZ, NKT cells then migrate further into the BCZ where cognate B cell-NKT interactions occur. It is likely that in a situation involving glycolipid and TCR-dependent activation of NKT cells, NKT cells enter the BCZ to provide cognate B cell help directly in the germinal centre.

We observed that the majority of NKT cells are located within the medulla of the thymus, which aligns with a previous study [18]. It is known that an interdependency exists between medullary thymic epithelial cells (mTEC) and thymocyte development [53], including a key role for NKT cells via RANKL and IL-13R

[37,54]. We intended to investigate whether Jα18$^{-/-}$ mice, which lack type I but retain type II NKT cells, also developed medullary holes, which would discriminate between the role of these two NKT cell subsets in regulating thymic emigration. However, we were unable to detect an increase in medullary holes in either CD1d$^{-/-}$ or Jα18$^{-/-}$ thymuses, on either B6 or BALB/c strain backgrounds. It is unclear why our observations differ from those previously published but given the influence of gut microbiota on NKT cells [55–57] it is possible that differences in gut microbiome of our mice compared to those used in the previous study may be responsible. Further studies will be required to elucidate the apparent conflict between these data reported here and those reported previously.

We have also demonstrated the *in situ* localisation of MAIT cells in spleen and lymph node with MR1-5-OP-RU tetramer and CD3 co-staining. Because MAIT cells are very rare in mice [41] we first used Vα19 TCR transgenic mice where these cells are more abundant and easier to detect. This reassured us that we were indeed able to detect MAIT cells in situ, although the scarcity of these cells in non-transgenic mice remains an obstacle to studying these cells in situ. However, through analysis of many sections from many mice, with appropriate controls including irrelevant Ac-6-FP loaded MR1 tetramer and MR1$^{-/-}$ mice, we were able to determine that MAIT cells appear to occupy different locations to NKT cells. For example, in contrast to NKT cells, in non-TCR transgenic mice, most MAIT cells were located outside the TCZ in spleen, which may result from differential expression of chemokine receptors. It is known that MAIT cells express CXCR6 and a subset expresses CCR9, which correlates with their well-known association with mucosal tissues, but not the TCZ homing chemokine CCR7 [41,58]. Conversely, of the NKT subsets, NKT2 cells have a greater expression of CCR7 [59,60]. As such, it is possible that the MAIT cells detected in the spleen are simply passing through the organ to other peripheral organs, while NKT2 cells are directed to TCZ. Alternatively, it is possible that MAIT cells are fulfilling a function in the RP and that the majority MAIT cells are expressing similar chemokine receptors as NKT1 cells and as such are directed to similar locations. The RP provides an environment to quickly scan for blood borne antigens [61], which may place RP-MAIT cells in a prime position to quickly respond to these antigens. Indeed, MAIT cells are important in the control of many bacterial infections (reviewed in [5]) including the control of blood borne infections such as *E. coli* and *M. absceccus* [62]. MAIT cells were also clearly observed in the thymus, mostly medulla but occasionally in cortext, of Vα19 transgenic mice, thus similar to NKT cells in their distribution. While rare examples of MR1 tetramer staining of CD3 + cells were also seen in the thymic cortex of wildtype mice, we remain cautious about overinterpreting these data because there were also rare instances of MR1 tetramer staining in negative controls on the non Vα19 transgenic mice. These may reflect rare T cells that express a TCR with the ability to bind to MR1, even in the absence of MR1-dependent intrathymic selection.

Taken together, this study demonstrates the use of CD1d and MR1 tetramers to detect NKT and MAIT cells in situ, respectively, and highlights the power of this technique when used in conjunction with TCR co-stains as well as appropriate tetramer and tissue controls. This approach should provide valuable insight into the function of these cells in different immunological and disease related settings.

Methods

Animal Models

BALB/c WT, BALB/c.Jα18$^{-/-}$, BALB/c.CD1d$^{-/-}$, B6 WT, B6.Jα18$^{-/-}$, B6.CD1d$^{-/-}$, B6.MR1$^{-/-}$, Vα19Tg and NOD were housed in Peter Doherty Institute Biological Research Facility (PDI BRF, Melbourne, Victoria, Australia) and either purchased from the PDI BRF or Animal Resource Centre (Perth, Western Australia, Australia). B6-MAIT$_{CAST}$ WT and B6-MAIT$_{CAST}$.MR1$^{-/-}$ (kindly supplied by Olivier Lantz, Institut Curie, Paris France) house in the Peter MacCallum Cancer Centre animal facility. Male or female mice 6–12 weeks of age, matched to age and sex, were housed and experiments performed in accordance to the relevant guidelines and regulations and under approval of the University of Melbourne Animal Ethics Committee (ethics number 1914739) or Peter MacCallum Cancer Centre animal ethics committee (ethics number E582). All experiments were carried out in compliance with the ARRIVE guidelines.

Chemical synthesis of MAIT cell antigen

5-OP-RU (5-(2-oxoethylideneamino)-6-d-ribitylaminouracil) was synthesised as previously detailed [63], by combining 5-A-RU (5-amino-6-d-ribitylaminouracil) and methylglyoxal in DMSO-d_6, where it is very stable.

Tetramer production

Recombinant mouse CD1d-α-GalCer and CD1d/GD3 were generated as previously described [64]. Purified mouse CD1d-biotin was incubated with PBS-44 C24:1 α-GalCer analogue (a gift from P. Savage, Brigham Young University, Provo, UT) or GD3 (Matreya LLC) at a 1:6 (monomer:ligand) molar ratio overnight at room temperature. Mouse MR1-5-OP-RU and MR1/Ac-6-FP tetramers were generated from purified recombinant mouse MR1 monomers as previously described [3,65]. The loaded CD1d or MR1 were tetramerised with the sequential addition (1/5 required volume) of unlabelled streptavidin, streptavidin-PE (BD) or streptavidin-FITC (BD) in 1/8 volume lots and a series of 10min incubations at 4^{o}C.

In vivo antigen stimulation

To stimulate NKT cells, male BALB/c mice 6–8 weeks of age were injected intraperitoneally with 2 μg α-GalCer (KRN7000, C26:0, Alexis Biochemicals) or with PBS alone. On days 3 and 5 post infection the mice were killed by CO_2 asphyxia, liver was perfused with PBS via the portal vein and livers and spleens were removed.

To stimulate MAIT cells, B6-MAIT$_{CAST}$ mice 6–12 weeks of age were treated intranasally with 50 μl of 232.4 μM synthetic 5-OP-RU or with PBS alone on days 0, 1, 2 and 4. On day 6 the mice were killed by cervical dislocation and the heart was perfused with 5ml PBS prior to the removal of mediastinal lymph node.

Mice were randomised by simple randomisation and blindly allocated to groups by animal house staff prior to assignment. Once allocated, no mice were excluded for analysis.

Cell suspensions

Thymus and spleen cell suspensions were prepared by gentle mechanical disruption of the tissues through 40µm nylon cell strainer into ice-cold FACS buffer (PBS with 2% FBS), treated with red blood cell lysis buffer (Sigma Aldrich) then resuspended in FACS buffer. Suspensions of hepatic leukocytes were prepared by gentle mechanical disruption of the liver through 40µm nylon cell strainer into ice-cold FACS buffer. To purify lymphocytes, cell suspensions were centrifuged in 33% Percoll (GE healthcare) and treated with red blood cell lysis buffer before resuspending in FACS buffer.

Flow cytometry

Cells were then incubated with 7-aminoactinomycin D (7-AAD, Thermo Fisher) plus antibodies against: mouse TCRβ (H57-597, BioLegend), B220 (RA3-6B2, BioLegend, BD BioSciences), CD19 (1D3, BD BioSciences), CD4 (RM4-5, BioLegend), mouse CD1d/α-GalCer (produced in house), Each reagent was titrated to determine the optimal dilution factor. All data were acquired on an LSR Fortessa™ II (BD), and analysed with FACSDiva and FlowJo (BD) software. All samples were gated on lymphocytes and with exclusion of doublets and dead cells using forward and side scatter area, forward scatter area and height and viability dye parameters, respectively.

Immunohistology

Mouse tissues were harvested and snap frozen in Optimal Cutting Temperature (OCT, Tissue-Tek) and 6 to 9 µm sections cut. Before removal, mice were perfused with PBS and lungs were inflated with 33% OCT and PBS solution. Sections were treated with 100% acetone (pre-chilled to -20^{o}C,) for 10 min at room temperature and air dried. Sections were blocked with 2% Bovine Serum Albumin (BSA, Sigma-Aldrich) and 10% normal mouse sera, and 10% normal goat, rat and/or donkey sera (Thermo Fisher Scienctific) as required depending on the primary, secondary or tertiary antibodies used, for 1 hour at room temperature. Sections were stained with various combinations of primary (anti-CD3 (500A2, eBiosciences), anti-CD4 (RM4.5, eBiosciences), anti-CD205 (NLDC-145, BioLegend) and anti-cytokeratin-5 (K5, EP1601Y, Abcam)) or labelled antibodies (anti-TCRβ AF647 (H57-597, BioLegend), anti-CD3 AF594 or AF647 (17A2, BioLegend), anti-CD4 AF488 (RM4.5, BD and BioLegend), anti-B220 Pacific Blue (RA3-6B2, BioLegend), anti-CD11c AF488 (N418, BioLegend), anti-CD11b biotin (M1/70, BioLegend), anti-MHC-II AF700 (M5/114.15.2, BioLegend), and CD31 AF647 (MEC13.3, BioLegend)) for 30min at room temperature. Where required, sections were then stained with streptavidin AF680 (Thermo Fisher Scientific), donkey anti-rat AF568 (Thermo Fisher Scientific) or goat anti-hamster AF568 (Thermo Fisher Scientific) secondary polyclonal antibodies with 10% normal mouse serum and 2% BSA diluted in PBS for 30min at room temperature. While the donkey and goat antibodies were cross absorbed to various species' Ig including mouse and rat by the manufacturer, the mixture of secondary antibody, normal mouse serum and BSA was made 30min prior to use to allow for additional absorption of potential mouse Ig binding sites. When required, sections were counter stained with DAPI (Thermo Fisher Scientific). All reagents were titrated to determine the optimal dilution factor. Slides were mounted with ProLong Gold Antifade (Thermo Fisher Scientific) and left to cure overnight before imaging.

When staining with either CD1d or MR1 tetramers, the following steps were also included. CD1d/GD3 or MR1/Ac-6-FP tetramer without a conjugated fluorochrome (20µg/mL) was included in the block, followed with biotin blocking solution (Thermo Fisher Scientific), as per manufacturer's instructions. Sections were then stained with 16µg/mL PE or FITC labelled CD1d tetramers loaded with α-GalCer, GD3 or unloaded and/or PE labelled MR1 tetramers loaded with 5-OP-RU or Ac-6-FP, for 30min 4^{o}C. Sections were fixed with 1% Paraformaldehyde (Electron Microscopy Sciences) for 30min at room temperature followed by treatment with 50µM NH_4Cl (Sigma-Aldrich) for 10min at room temperature. Sections then stained with polyclonal rabbit or goat anti-PE and/or polyclonal rabbit anti-FITC (Thermo Fisher Scientific) with 10% normal mouse serum. This was followed by a secondary stain as above with goat anti-rabbit-AF555, donkey anti-goat-AF555 or donkey anti-rabbit-AF488 (Thermo Fisher Scientific).

Z-stack, 2x2 or 3x3 tiled images with 76.9 nm lateral and 400 nm axial voxel size and 1024x1024 voxel density were recorded on either LMS-700, LSM-710 or LSM780 laser scanning inverted confocal microscopes with a 20x/0.8NA objective (Zeiss). Fluorochromes were excited with 405, 488, 561 and 633 nm lasers. The tiles of each image were stitched together after acquisition.

Bioimage analysis and histo-cytometry

Spectral unmixing was performed with Zen software. Image deconvoluted was performed with Huygens Professional (Scientific Volume Imaging) and images analysed with FIJI/ImageJ and Imaris (Oxford Instruments) software. Compensation post deconvolution was performed with the Spectral Unmixing FIJI/Image J plugin [66]. Colocalization analysis and calculation of Pearson correlation coefficients were performed with the Imaris Colocalization module with intensity thresholds set for each analysed channel based on negative controls for each stain. Max intensity was performed to flatten the z-stacks and all thresholding was performed in FIJI/ImageJ. Where image intensity changes were performed to reduce background autofluorescence and increase visual clarity, this was equally preformed across all images from test and control groups within an experiment.

To count the number of NKT cells within 100 µm of thymic CMJ, a FIJI/Image J script (see supplementary) was used. The location of NKT cells were manually determined and the region of interest (ROI) outlining the CMJ was manually drawn at the CD205 and K5 interface for each image. For analysis of thymic medullary voids, the medullary ROI were determined for each image based on the K5 and DAPI stain. A FIJI/Image J script (see supplementary) was used to determine, outline and measure the thymic medullary voids. These were defined in the script as continuous areas within the thymic medulla ROI > 5000µm^2 lacking in K5 stain.

Histocytometry was performed in a similar way to that described previously [43]. Briefly, once spectral unmixing, deconvolution and compensation were complete, cell segmentation was performed based on the DAPI stain with the Imaris surface rendering module. The mean channel intensity values, area, volume and x, y, z position data from each segmented surface were exported into FlowJo for cytometry analysis. The segmented surfaces were separated into the various cell types in Flowjo, which were plotted back to the original cell surfaces in Imaris and used to mask on specific channels to visually represent the cell

types (B220 for B cells, CD3 for T cells, CD1d-α-GalCer tetramer for NKT cells, CD11c for DCs, and CD11b for Macrophages, while DAPI was used for miscellaneous cell population).

Statistics

Prism software (Graphpad) was used for t test and ANOVA statistical analysis, comparison tests and the generation of p values, * = $p < 0.05$, ** = $p < 0.01$ *** = $p < 0.005$, **** = $p < 0.001$.

Declarations

Data Availability

All datasets generated and/or analysed during this study are included in this published article and the supplementary information.

Acknowledgements

The authors wish to thank Sidonia Eckle and Lyudmila Kostenko for intellectual input and technical assistance, Ellie Cho for assistance in bioimage analysis and Olivier Lantz for kindly supplying B6-$MAIT_{CAST}$ mice. All image acquisition was performed on microscopes maintained by the Biological Optical Microscopy Platform (BOMP), The University of Melbourne. We acknowledge the support of an Australian Research Council (ARC) Centre of Excellence in Advanced Molecular Imaging (grant CE140100011) and the National Health and Medical Research Council (NHMRC) program grant (1113293); project grant (APP1125493); research fellowships (APP1117017; 1117766, 1136680).

Additional Information

JYWM, DPF and JMc are inventors on patents describing MR1 tetramers and MR1 ligands. All other authors have no conflicts of interest to declare.

Author Contributions

Conceptualisation DNJ and DIG; Experiments DNJ, EVP, SP, LEH, APU, JLH and SNM: Investigation and data analysis DNJ and EVP; Resources ZR, EVP, APU, JYWM, SNM, JMc, DPF, PKD, PAB, WRH and DIG; Original draft DNJ and DIG; editing EVP, APU, JYWM, JLH and WRH; All authors read and approved the final manuscript.

References

1. Godfrey, D. I., Uldrich, A. P., McCluskey, J., Rossjohn, J. & Moody, D. B. The burgeoning family of unconventional T cells. *Nature immunology*, **16**, 1114–1123 https://doi.org/10.1038/ni.3298 (2015).

2. Kawano, T. *et al.* CD1d-restricted and TCR-mediated activation of valpha14 NKT cells by glycosylceramides., **278**, 1626–1629 https://doi.org/10.1126/science.278.5343.1626 (1997).
3. Corbett, A. *et al.* T-cell activation by transitory neo-antigens derived from distinct microbial pathways. *Nature*, **509**, 361–365 (2014).
4. Eckle, S. B. *et al.* Recognition of Vitamin B Precursors and Byproducts by Mucosal Associated Invariant T Cells. *J Biol Chem*, **290**, 30204–30211 https://doi.org/10.1074/jbc.R115.685990 (2015).
5. Godfrey, D. I., Koay, H. F., McCluskey, J. & Gherardin, N. A. The biology and functional importance of MAIT cells. *Nature immunology*, **20**, 1110–1128 https://doi.org/10.1038/s41590-019-0444-8 (2019).
6. Crosby, C. M. & Kronenberg, M. Tissue-specific functions of invariant natural killer T cells. *Nature reviews*, **18**, 559–574 https://doi.org/10.1038/s41577-018-0034-2 (2018).
7. Lee, W. Y. *et al.* An intravascular immune response to Borrelia burgdorferi involves Kupffer cells and iNKT cells. *Nature immunology*, **11**, 295–302 (2010).
8. Geissmann, F. *et al.* Intravascular Immune Surveillance by CXCR6 + NKT Cells Patrolling Liver Sinusoids. *PLoS Biology*, **3**, e113–661 (2005).
9. Lee, W. Y. *et al.* Invariant natural killer T cells act as an extravascular cytotoxic barrier for joint-invading Lyme Borrelia. *Proceedings of the National Academy of Sciences* **111**, 13936–13941, doi:10.1073/pnas.1404769111 (2014).
10. Kastenmueller, W. *et al.* A Spatially-Organized Multicellular Innate Immune Response in Lymph Nodes Limits Systemic Pathogen Spread., **150**, 1235–1248 (2012).
11. Barral, P. *et al.* CD169 + macrophages present lipid antigens to mediate early activation of iNKT cells in lymph nodes. *Nature immunology*, **11**, 303–312 (2010).
12. Chang, P. P. *et al.* Identification of Bcl-6-dependent follicular helper NKT cells that provide cognate help for B cell responses. *Nature immunology*, **13**, 35–43 https://doi.org/10.1038/ni.2166 (2011).
13. Barral, P. *et al.* The location of splenic NKT cells favours their rapid activation by blood-borne antigen. *EMBO journal*, **31**, 2378–2390 (2012).
14. Werner, J. *et al.* Distribution of intrahepatic T, NK and CD3 + CD56 + NKT cells alters after liver transplantation: Shift from innate to adaptive immunity? *Transplant immunology*, **25**, 27–33 (2011).
15. Godfrey, D. I., MacDonald, H. R., Kronenberg, M., Smyth, M. J. & Van Kaer L. NKT cells: what's in a name? *Nature reviews*, **4**, 231–237 https://doi.org/10.1038/nri1309 (2004).
16. Thomas, S. *et al.* PLZF induces an intravascular surveillance program mediated by long-lived LFA-1-ICAM-1 interactions. *The Journal of experimental medicine*, **208**, 1179–1188 (2011).
17. King, I. L. *et al.* The mechanism of splenic invariant NKT cell activation dictates localization in vivo. *J Immunol*, **191**, 572–582 https://doi.org/10.4049/jimmunol.1300299 (2013).
18. Lee, Y. *et al.* Tissue-Specific Distribution of iNKT Cells Impacts Their Cytokine Response., **43**, 566–578 (2015).
19. Gaya, M. *et al.* Initiation of Antiviral B Cell Immunity Relies on Innate Signals from Spatially Positioned NKT Cells. *Cell* **172**, 517–533 e520, doi:10.1016/j.cell.2017.11.036 (2018).

20. Lynch, L. *et al.* Regulatory iNKT cells lack expression of the transcription factor PLZF and control the homeostasis of Treg cells and macrophages in adipose tissue. *Nature immunology*, **16**, 85–95 (2015).
21. Berglin, L. *et al.* In situ characterization of intrahepatic non-parenchymal cells in PSC reveals phenotypic patterns associated with disease severity. *PLoS One*, **9**, e105375 https://doi.org/10.1371/journal.pone.0105375 (2014).
22. Dusseaux, M. *et al.* Human MAIT cells are xenobiotic-resistant, tissue-targeted, CD161hi IL-17-secreting T cells., **117**, 1250–1259 https://doi.org/10.1182/blood-2010-08-303339 (2011).
23. Hegde, P. *et al.* Mucosal-associated invariant T cells are a profibrogenic immune cell population in the liver. *Nat Commun*, **9**, 2146 https://doi.org/10.1038/s41467-018-04450-y (2018).
24. Jeffery, H. C. *et al.* Biliary epithelium and liver B cells exposed to bacteria activate intrahepatic MAIT cells through MR1. *J Hepatol*, **64**, 1118–1127 https://doi.org/10.1016/j.jhep.2015.12.017 (2016).
25. Riva, A. *et al.* Mucosa-associated invariant T cells link intestinal immunity with antibacterial immune defects in alcoholic liver disease., **67**, 918–930 https://doi.org/10.1136/gutjnl-2017-314458 (2018).
26. Hiejima, E. *et al.* Reduced Numbers and Proapoptotic Features of Mucosal-associated Invariant T Cells as a Characteristic Finding in Patients with Inflammatory Bowel Disease. *Inflamm Bowel Dis*, **21**, 1529–1540 https://doi.org/10.1097/MIB.0000000000000397 (2015).
27. Haga, K. *et al.* MAIT cells are activated and accumulated in the inflamed mucosa of ulcerative colitis. *J Gastroenterol Hepatol*, **31**, 965–972 https://doi.org/10.1111/jgh.13242 (2016).
28. Won, E. J. *et al.* Clinical relevance of circulating mucosal-associated invariant T cell levels and their anti-cancer activity in patients with mucosal-associated cancer. *Oncotarget*, **7**, 76274–76290 https://doi.org/10.18632/oncotarget.11187 (2016).
29. Serriari, N. E. *et al.* Innate mucosal-associated invariant T (MAIT) cells are activated in inflammatory bowel diseases. *Clin Exp Immunol*, **176**, 266–274 https://doi.org/10.1111/cei.12277 (2014).
30. Kuric, E. *et al.* No Evidence for Presence of Mucosal-Associated Invariant T Cells in the Insulitic Lesions in Patients Recently Diagnosed with Type 1 Diabetes. *Am J Pathol*, **188**, 1744–1748 https://doi.org/10.1016/j.ajpath.2018.04.009 (2018).
31. Abrahamsson, S. V. *et al.* Non-myeloablative autologous haematopoietic stem cell transplantation expands regulatory cells and depletes IL-17 producing mucosal-associated invariant T cells in multiple sclerosis., **136**, 2888–2903 https://doi.org/10.1093/brain/awt182 (2013).
32. Salou, M. *et al.* Neuropathologic, phenotypic and functional analyses of Mucosal Associated Invariant T cells in Multiple Sclerosis. *Clin Immunol*, **166–167**, 1–11 https://doi.org/10.1016/j.clim.2016.03.014 (2016).
33. Willing, A. *et al.* CD8(+) MAIT cells infiltrate into the CNS and alterations in their blood frequencies correlate with IL-18 serum levels in multiple sclerosis. *European journal of immunology*, **44**, 3119–3128 https://doi.org/10.1002/eji.201344160 (2014).
34. Wang, H. *et al.* MAIT cells protect against pulmonary Legionella longbeachae infection. *Nat Commun*, **9**, 3350 https://doi.org/10.1038/s41467-018-05202-8 (2018).

35. Trottein, F., Paget, C. & Natural Killer, T. Cells and Mucosal-Associated Invariant T Cells in Lung Infections. *Front Immunol*, **9**, 1750 https://doi.org/10.3389/fimmu.2018.01750 (2018).
36. Matsuda, J. L., Mallevaey, T., Scott-Browne, J. & Gapin, L. CD1d-restricted iNKT cells, the 'Swiss-Army knife' of the immune system. *Curr Opin Immunol*, **20**, 358–368 https://doi.org/10.1016/j.coi.2008.03.018 (2008).
37. White, A. J. *et al.* A type 2 cytokine axis for thymus emigration. *J Exp Med*, **214**, 2205–2216 https://doi.org/10.1084/jem.20170271 (2017).
38. Savino, W., Boitard, C., Bach, J. F. & Dardenne, M. Studies on the thymus in nonobese diabetic mouse. I. Changes in the microenvironmental compartments. *Lab Invest*, **64**, 405–417 (1991).
39. Koay, H. F. *et al.* A three-stage intrathymic development pathway for the mucosal-associated invariant T cell lineage. *Nature immunology*, **17**, 1300–1311 https://doi.org/10.1038/ni.3565 (2016).
40. Treiner, E. *et al.* Selection of evolutionarily conserved mucosal-associated invariant T cells by MR1. *Nature*, **422**, 164–169 https://doi.org/10.1038/nature01433 (2003).
41. Rahimpour, A. *et al.* Identification of phenotypically and functionally heterogeneous mouse mucosal-associated invariant T cells using MR1 tetramers. *J Exp Med*, **212**, 1095–1108 https://doi.org/10.1084/jem.20142110 (2015).
42. Matsuda, J., Mallevaey, T., Scott Browne, J. & Gapin, L. CD1d-restricted iNKT cells, the Swiss-Army knife of the immune system. *Current opinion in immunology*, **20**, 358–368 (2008).
43. Gerner, M. Y., Kastenmuller, W., Ifrim, I., Kabat, J. & Germain, R. N. Histo-Cytometry: A Method for Highly Multiplex Quantitative Tissue Imaging Analysis Applied to Dendritic Cell Subset Microanatomy in Lymph Nodes., **37**, 364–376 https://doi.org/10.1016/j.immuni.2012.07.011 (2012).
44. McWilliam, H. E. G. *et al.* Endoplasmic reticulum chaperones stabilize ligand-receptive MR1 molecules for efficient presentation of metabolite antigens. *Proc Natl Acad Sci U S A*, **117**, 24974–24985 https://doi.org/10.1073/pnas.2011260117 (2020).
45. Cui, Y. *et al.* Mucosal-associated invariant T cell-rich congenic mouse strain allows functional evaluation. *J Clin Invest*, **125**, 4171–4185 https://doi.org/10.1172/JCI82424 (2015).
46. Hammond, K. J. L. *et al.* CD1d-Restricted NKT Cells: An Interstrain Comparison. *The Journal of Immunology*, **167**, 1164–1173 https://doi.org/10.4049/jimmunol.167.3.1164 (2001).
47. Richardson, D. S. & Lichtman, J. W. Clarifying Tissue Clearing., **162**, 246–257 https://doi.org/10.1016/j.cell.2015.06.067 (2015).
48. Lee, Y. J., Holzapfel, K. L., Zhu, J., Jameson, S. C. & Hogquist, K. A. Steady-state production of IL-4 modulates immunity in mouse strains and is determined by lineage diversity of iNKT cells. *Nature immunology*, **14**, 1146–1154 https://doi.org/10.1038/ni.2731 (2013).
49. Brennan, P. J., Brigl, M. & Brenner, M. B. Invariant natural killer T cells: an innate activation scheme linked to diverse effector functions. *Nature Reviews Immunology*, **13**, 101–117 https://doi.org/10.1038/nri3369 (2013).

50. Leadbetter, E. A. *et al.* NK T cells provide lipid antigen-specific cognate help for B cells. *Proc Natl Acad Sci U S A*, **105**, 8339–8344 https://doi.org/10.1073/pnas.0801375105 (2008).
51. Bai, L. *et al.* Natural killer T (NKT)-B-cell interactions promote prolonged antibody responses and long-term memory to pneumococcal capsular polysaccharides. *Proc Natl Acad Sci U S A*, **110**, 16097–16102 https://doi.org/10.1073/pnas.1303218110 (2013).
52. Barral, P. *et al.* B cell receptor-mediated uptake of CD1d-restricted antigen augments antibody responses by recruiting invariant NKT cell help in vivo. *Proc Natl Acad Sci U S A*, **105**, 8345–8350 https://doi.org/10.1073/pnas.0802968105 (2008).
53. van Ewijk, W., Shores, E. W. & Singer, A. Crosstalk in the mouse thymus. *Immunol Today*, **15**, 214–217 https://doi.org/10.1016/0167-5699(94)90246-1 (1994).
54. White, A. J. *et al.* An essential role for medullary thymic epithelial cells during the intrathymic development of invariant NKT cells. *J Immunol*, **192**, 2659–2666 https://doi.org/10.4049/jimmunol.1303057 (2014).
55. Wingender, G. *et al.* Intestinal microbes affect phenotypes and functions of invariant natural killer T cells in mice., **143**, 418–428 https://doi.org/10.1053/j.gastro.2012.04.017 (2012).
56. An, D. *et al.* Sphingolipids from a symbiotic microbe regulate homeostasis of host intestinal natural killer T cells., **156**, 123–133 https://doi.org/10.1016/j.cell.2013.11.042 (2014).
57. Olszak, T. *et al.* Microbial exposure during early life has persistent effects on natural killer T cell function., **336**, 489–493 https://doi.org/10.1126/science.1219328 (2012).
58. Toubal, A., Nel, I., Lotersztajn, S. & Lehuen, A. Mucosal-associated invariant T cells and disease. *Nature reviews*, **19**, 643–657 https://doi.org/10.1038/s41577-019-0191-y (2019).
59. Cohen, N. R. *et al.* Shared and distinct transcriptional programs underlie the hybrid nature of iNKT cells. *Nature immunology*, **14**, 90–99 https://doi.org/10.1038/ni.2490 (2013).
60. Engel, I. *et al.* Innate-like functions of natural killer T cell subsets result from highly divergent gene programs. *Nature immunology*, **17**, 728–739 https://doi.org/10.1038/ni.3437 (2016).
61. Mebius, R. E. & Kraal, G. Structure and function of the spleen. *Nature reviews*, **5**, 606–616 https://doi.org/10.1038/nri1669 (2005).
62. Le Bourhis, L. *et al.* Antimicrobial activity of mucosal-associated invariant T cells. *Nature immunology*, **11**, 701–708 https://doi.org/10.1038/ni.1890 (2010).
63. Mak, J. Y. *et al.* Stabilizing short-lived Schiff base derivatives of 5-aminouracils that activate mucosal-associated invariant T cells. *Nat Commun*, **8**, 14599 https://doi.org/10.1038/ncomms14599 (2017).
64. Pellicci, D. *et al.* Differential Recognition of CD1d-Î±-Galactosyl Ceramide by the VÎ²8.2 and VÎ²7 Semi-invariant NKT T Cell Receptors., **31**, 47–59 (2009).
65. Eckle, S. B. G. *et al.* A molecular basis underpinning the T cell receptor heterogeneity of mucosal-associated invariant T cells. *The Journal of experimental medicine*, https://doi.org/10.1084/jem.20140484 (2014).

66. Gammon, S. T., Leevy, W. M., Gross, S., Gokel, G. W. & Piwnica-Worms, D. Spectral unmixing of multicolored bioluminescence emitted from heterogeneous biological sources. *Anal Chem*, **78**, 1520–1527 https://doi.org/10.1021/ac051999h (2006).

Figures

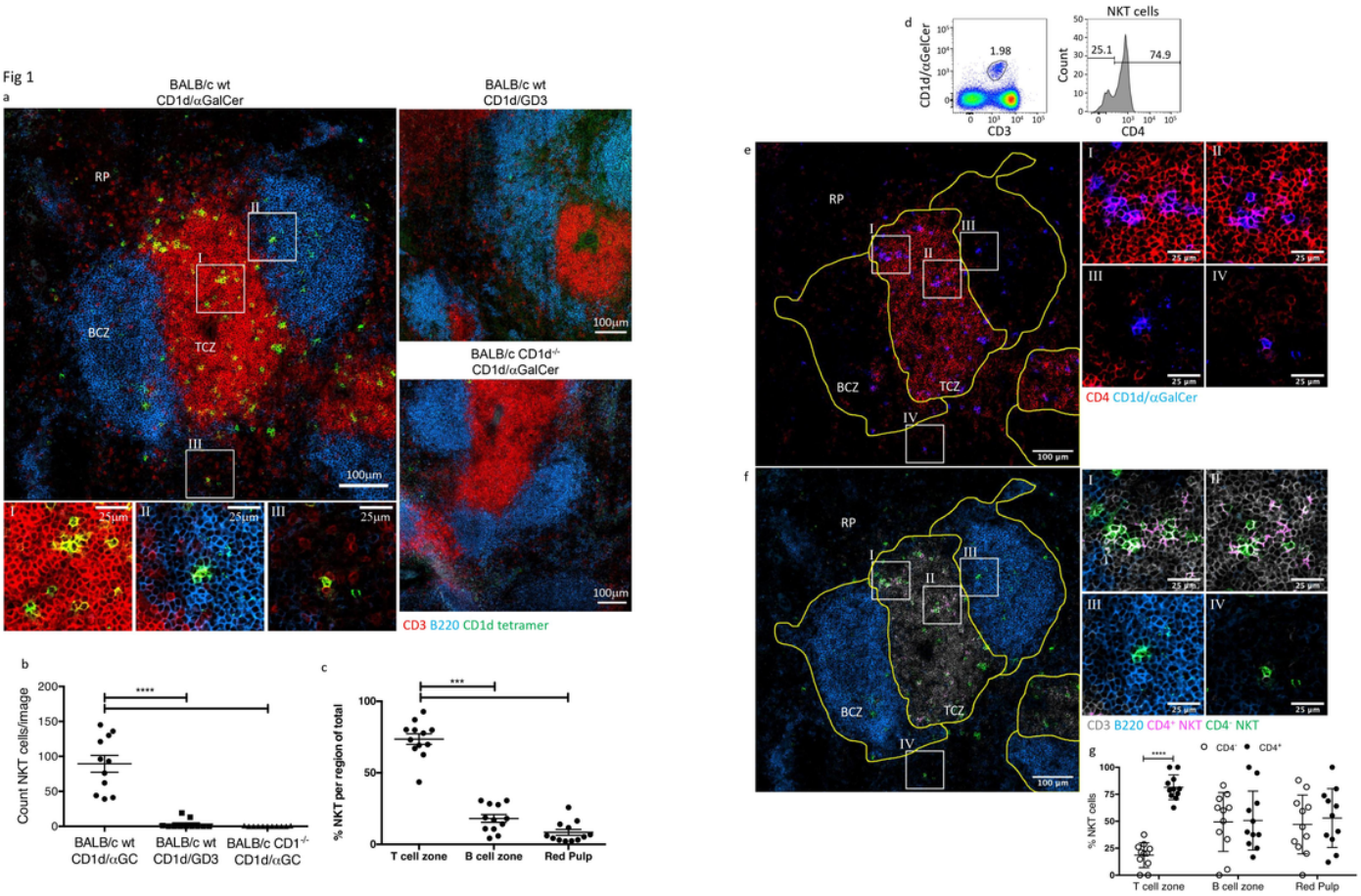

Figure 1

Please See the Supplemental Files section for the complete figure caption

Fig 2

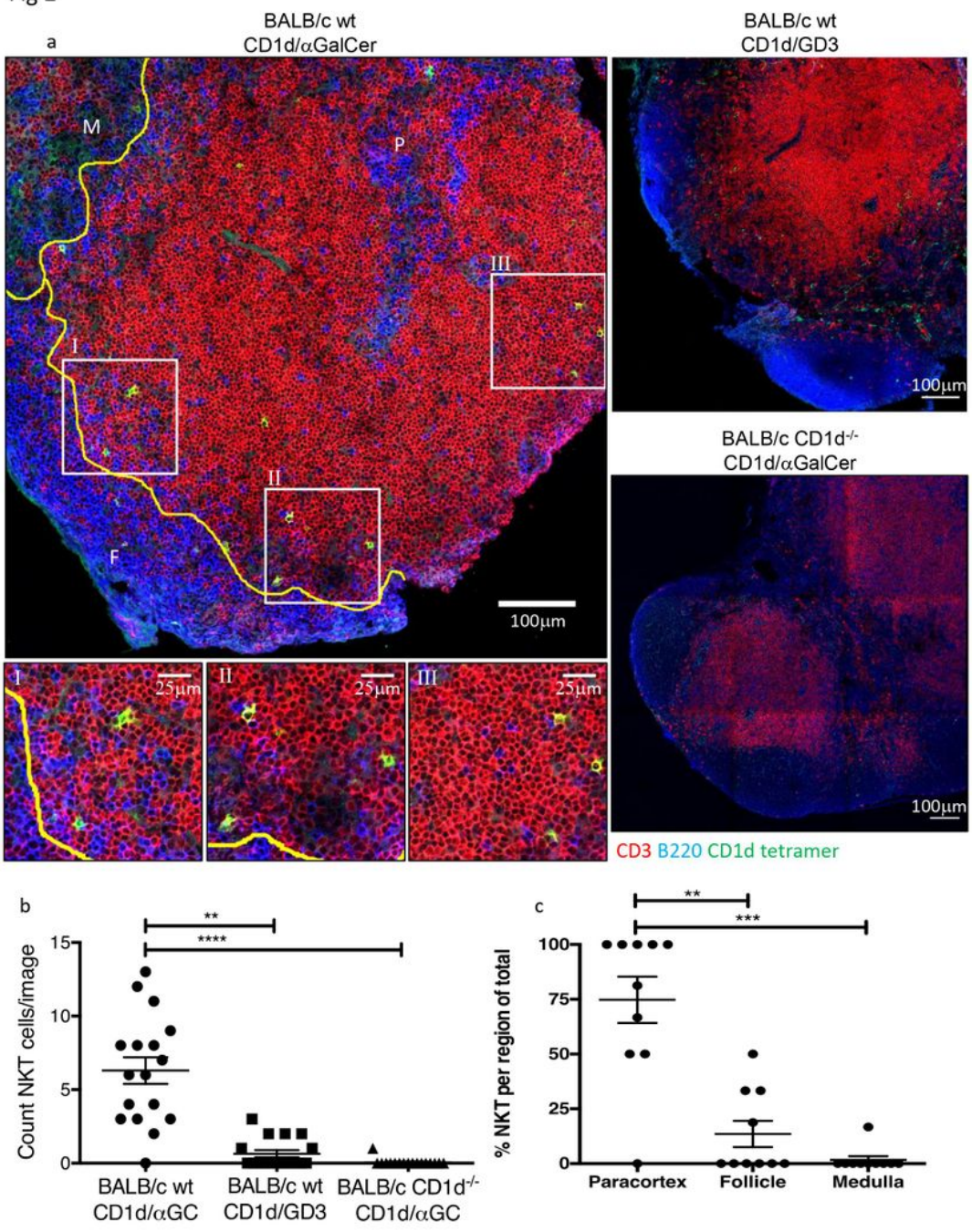

Figure 2

Please See the Supplemental Files section for the complete figure caption

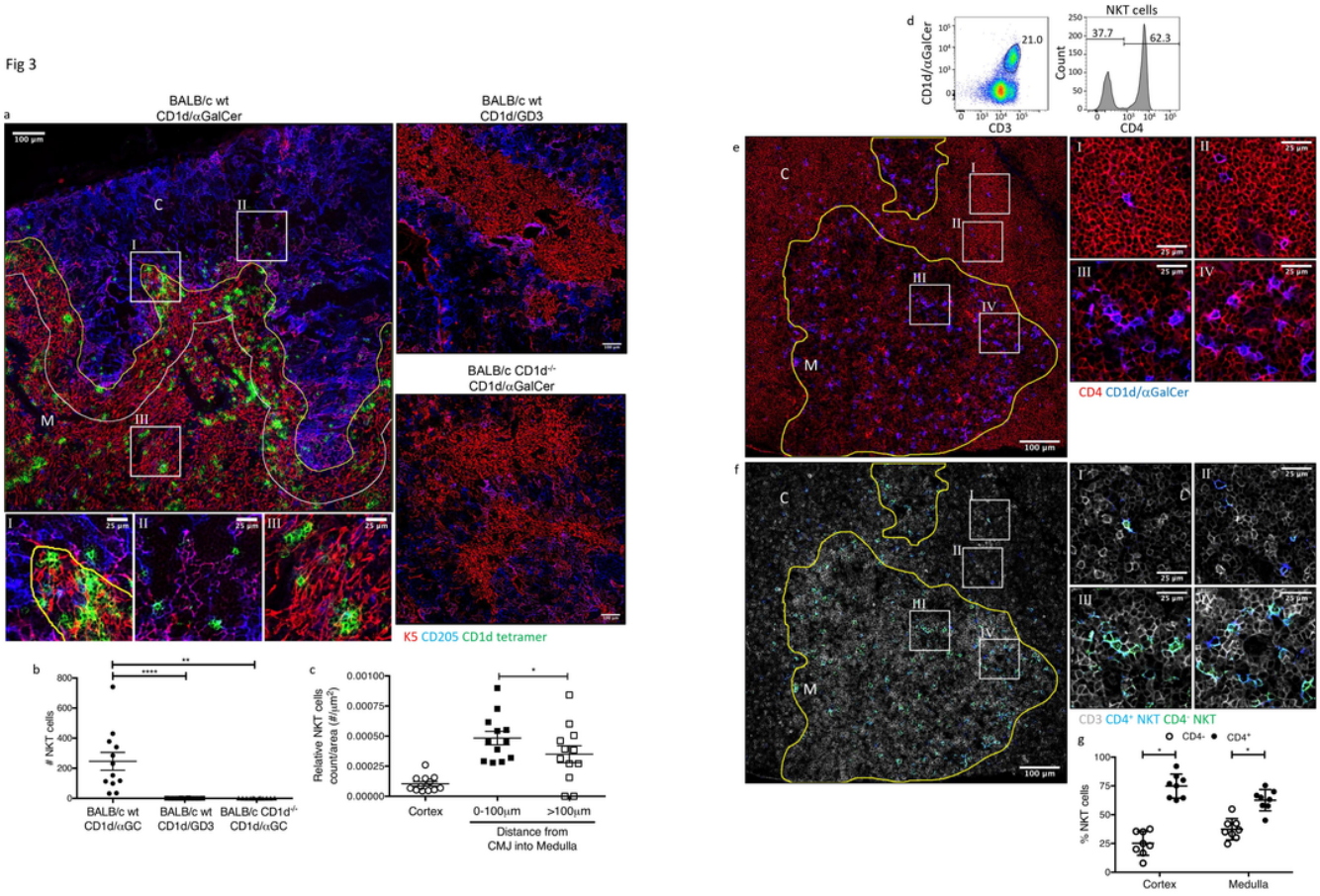

Figure 3

Please See the Supplemental Files section for the complete figure caption

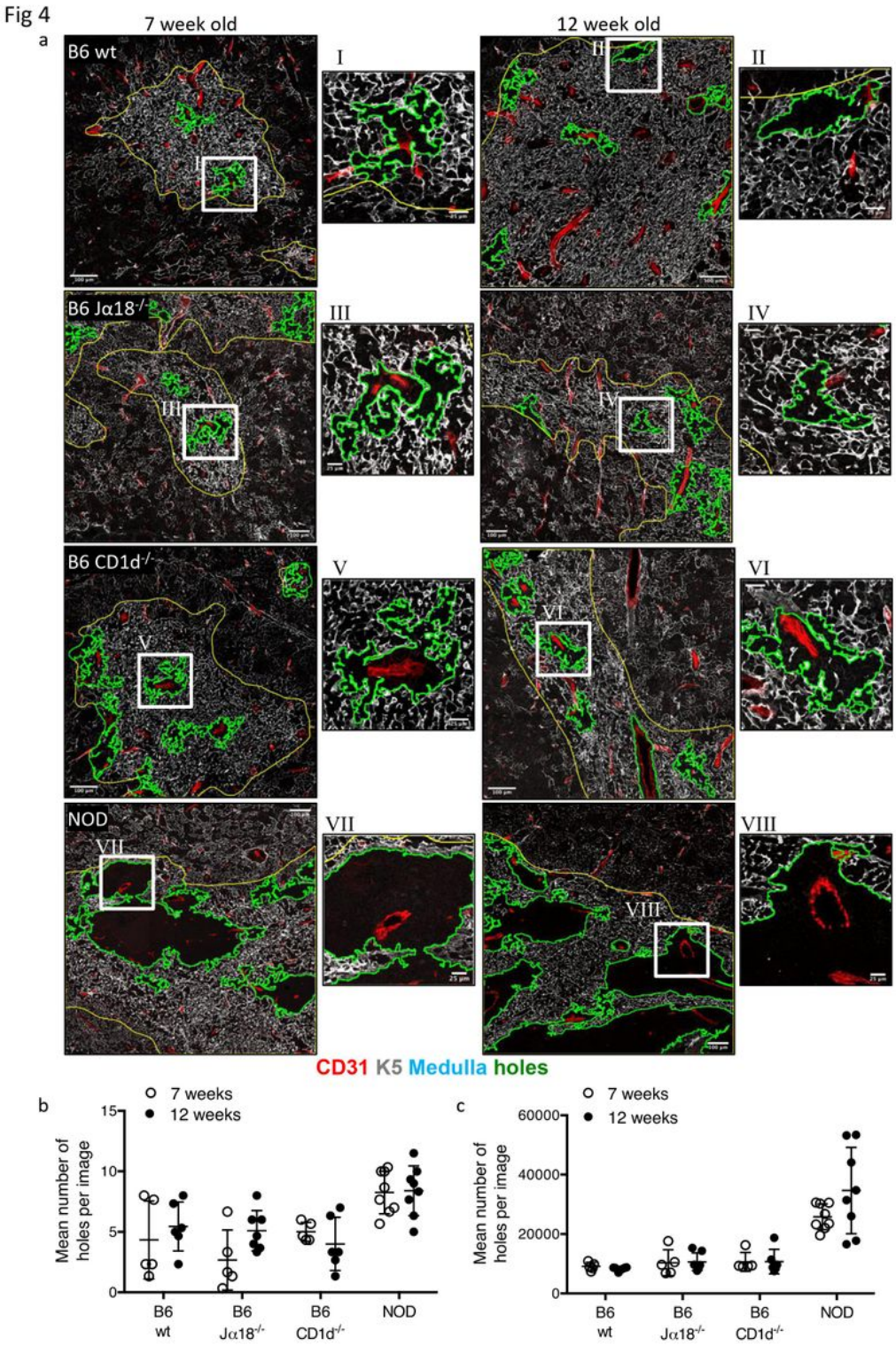

Figure 4

Please See the Supplemental Files section for the complete figure caption

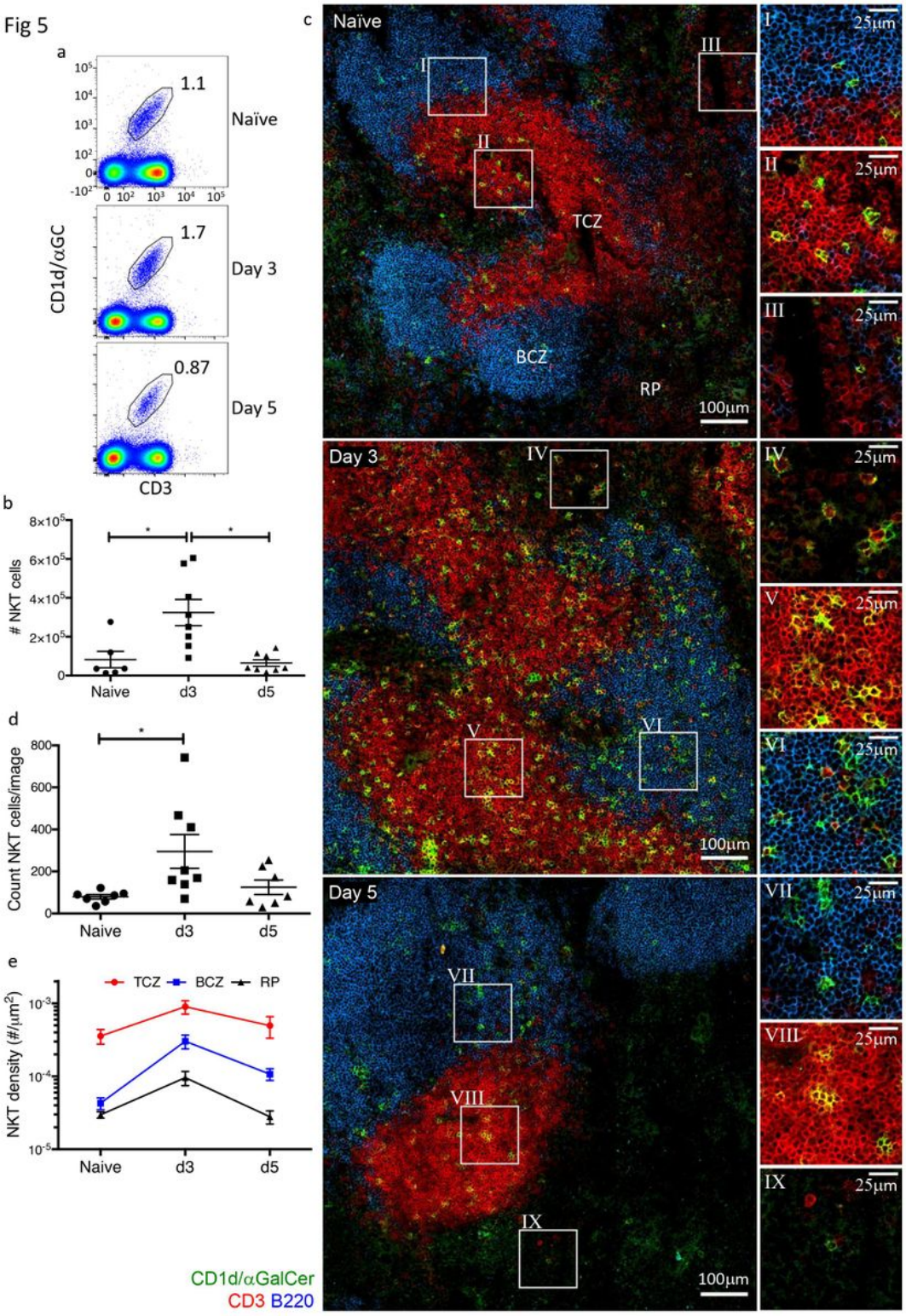

Figure 5

Please See the Supplemental Files section for the complete figure caption

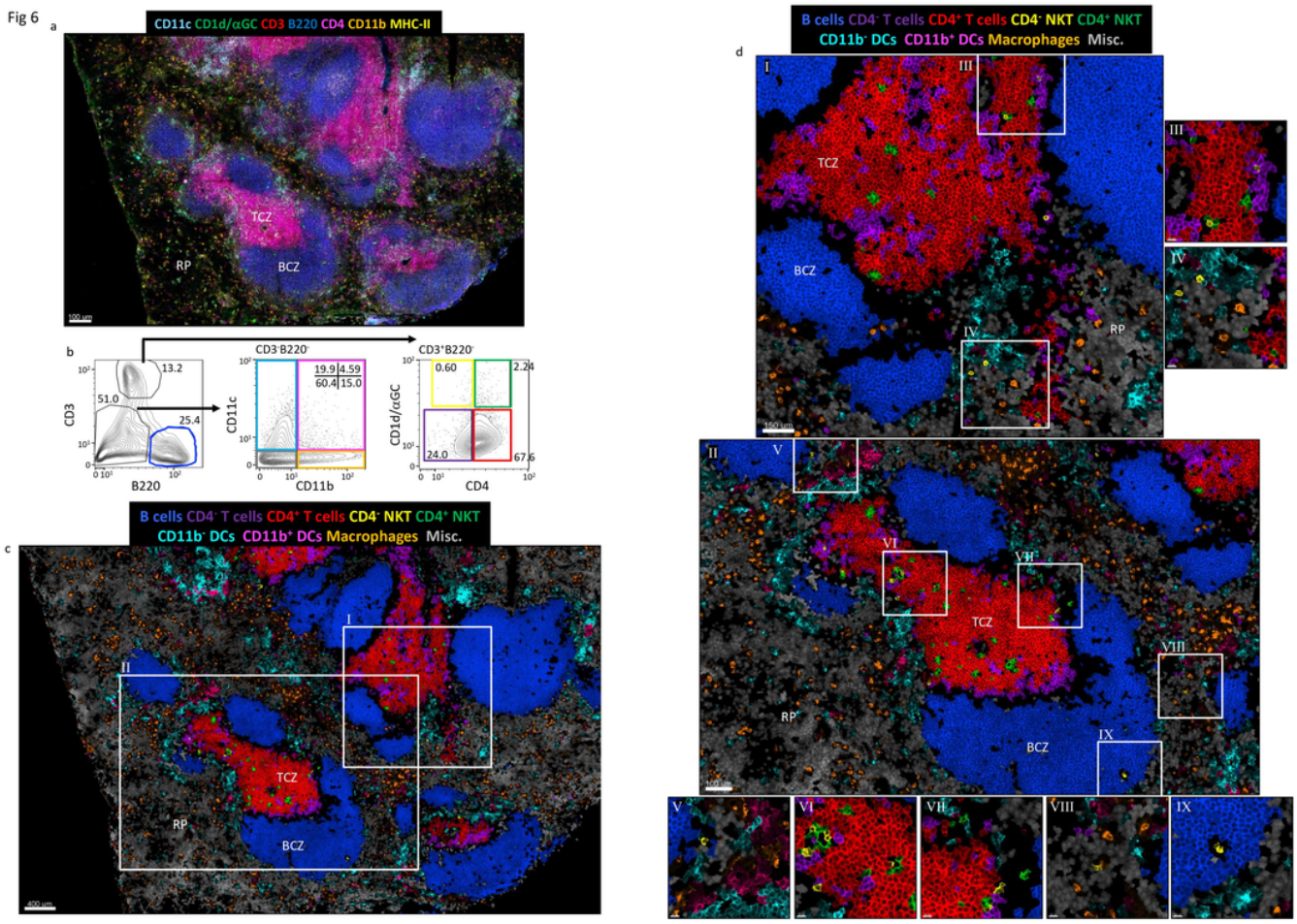

Figure 6

Please See the Supplemental Files section for the complete figure caption

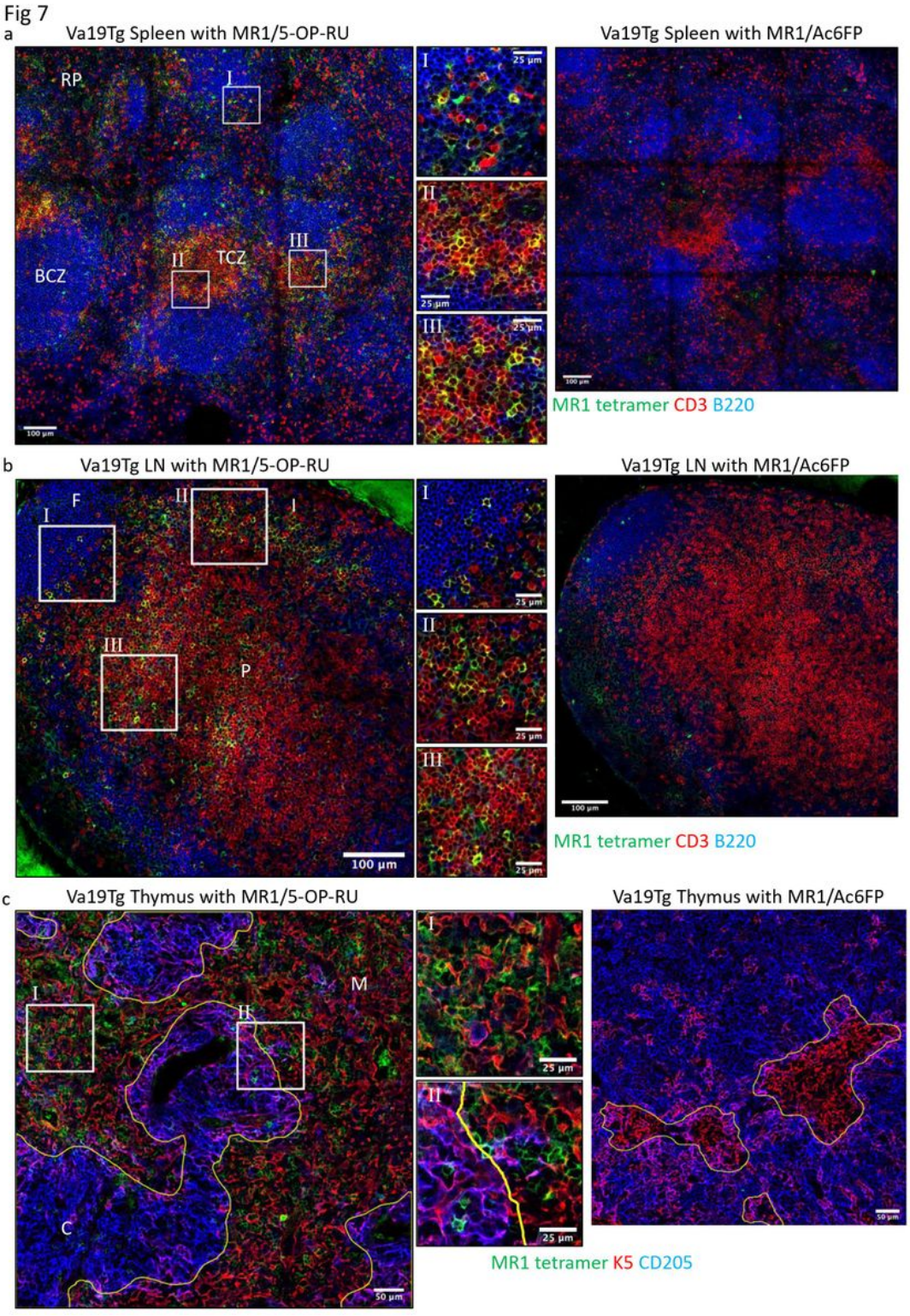

Figure 7

Please See the Supplemental Files section for the complete figure caption

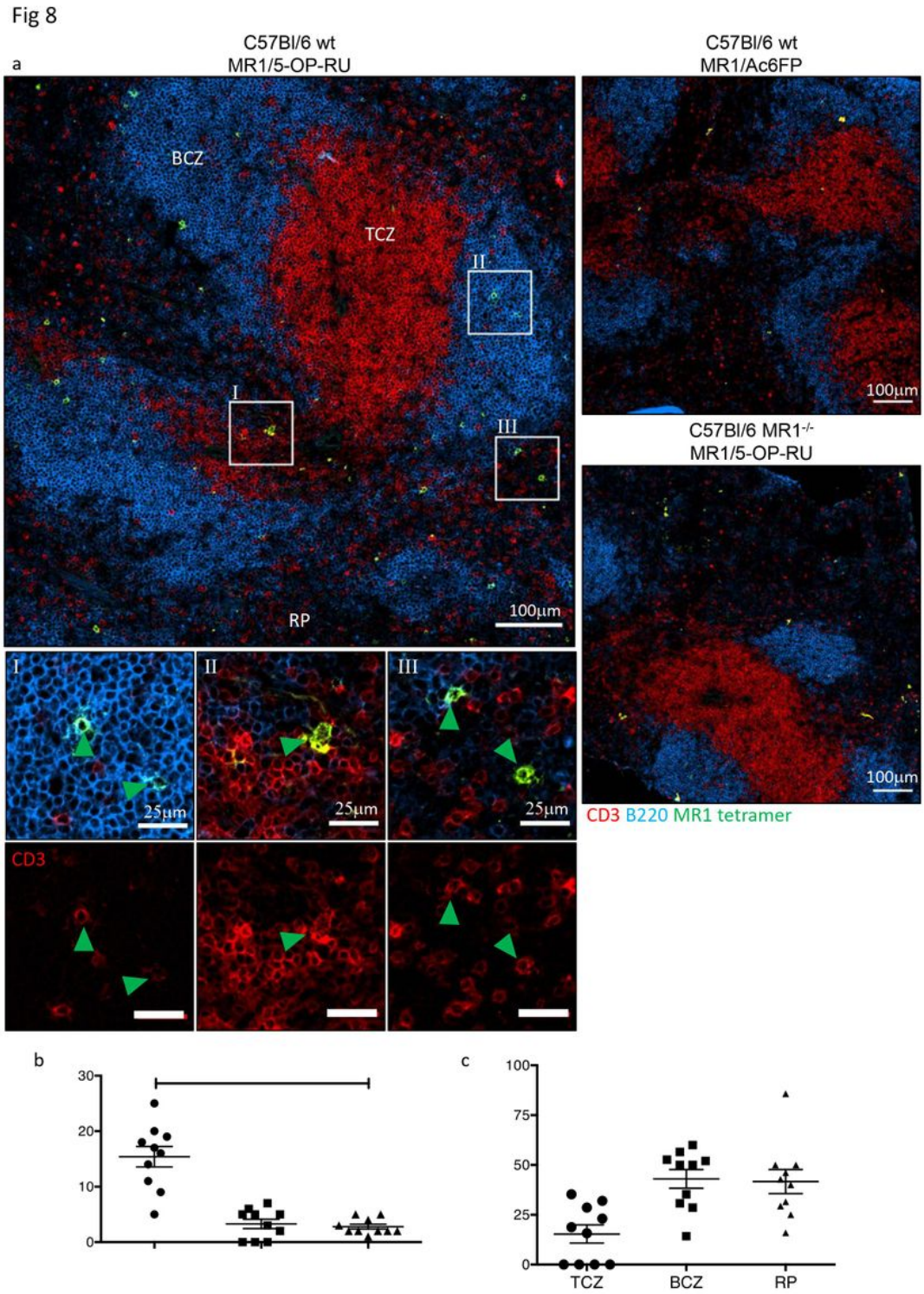

Figure 8

Please See the Supplemental Files section for the complete figure caption

Supplementary Files

This is a list of supplementary files associated with this preprint. Click to download.

- SupplementaryDifferentiallocationofNKTandMAITcellswithinlymphoidtissueDJohnson.pdf
- SupplementaryFiguresDifferentiallocationofNKTandMAITcellswithinlymphoidtissueDJohnson.pdf
- FigureLegends.docx